Submitted to: *Phys. Med. Biol.* **61** (2016) 5037–5050. ‡

Modeling of body tissues for Monte Carlo simulation of radiotherapy treatments planned with conventional x-ray CT systems

Nobuyuki Kanematsu, Taku Inaniwa and Minoru Nakao§

Department of Accelerator and Medical Physics, National Institute of Radiological Sciences, 4-9-1 Anagawa, Inage-ku, Chiba 263-8555, Japan

E-mail: kanematsu.nobuyuki@qst.go.jp

Abstract. In the conventional procedure for accurate Monte Carlo simulation of radiotherapy, a CT number given to each pixel of a patient image is directly converted to mass density and elemental composition, using their respective functions that have been calibrated specifically for the relevant x-ray CT system. We propose an alternative approach that is a conversion in two steps: the first from CT number to density and the second from density to composition. Based on the latest compilation of standard tissues for reference adult male and female phantoms, we sorted the standard tissues by mass density into groups and represented them by the averaged materials per group. With these representative tissues, we formulated polyline relations between mass density and each of electron density, stopping-power ratio and elemental densities. We also revised a procedure of stoichiometric calibration for CT-number conversion and demonstrated the two-step conversion method for a theoretically emulated CT system with hypothetical 80-keV photons. For the standard tissues, high correlation was generally observed between mass density and the other densities, excluding those of C and O for the light spongiosa tissues between 1.0 g/cm^3 and 1.1 g/cm^3 occupying 1% of the human body mass. The polylines fitted to the dominant tissues were generally consistent with similar formulations in the literature. The two-step conversion procedure was demonstrated to be practical and will potentially facilitate Monte Carlo simulation for treatment planning and for retrospective analysis of treatment plans with little impact on the management of planning CT systems.

PACS numbers: 87.55.D-, 87.55.K-, 87.57.Q-

Keywords: body tissue modeling, Monte Carlo simulation, radiation treatment planning, CT number calibration, stoichiometric analysis

§ Present address: Hiroshima High-Precision Radiotherapy Cancer Center, 3-2-2 Futabanosato, Higashi-ku, Hiroshima 732-0057, Japan

1. Introduction

In treatment planning (TP) for radiotherapy (RT), a patient body is commonly modeled to be made of H_2O of variable effective density (ED), which is an approximate concept for a physical interaction of interest. The ED is generally regarded as the relative electron density for energetic photons or as the stopping-power ratio for charged particles. Commonly, the patient model is derived from single-energy (SE) kilovoltage (kV) x-ray computed tomography (CT) with a selectable function to convert a CT number of each image pixel to an ED for RT. The standard approach to an accurate conversion function involves experimental x-ray modeling and stoichiometric analysis of standard body tissues to relate the CT number with the ED (Schneider *et al* 1996, Kanematsu *et al* 2003). To address multiple interactions in dose calculation for proton and ion RT, a two-step approach is often applied, in which a CT number is converted conventionally to a primary ED and then automatically to an interaction-specific secondary ED using a predefined invariant relation between the EDs (Fippel and Soukup 2004, Kanematsu *et al* 2012, Farace 2014, Kanematsu *et al* 2014, Inaniwa *et al* 2015a, 2015b, 2016).

With the advancement of computer technology, Monte Carlo (MC) simulation for the best achievable accuracy is becoming realistic. In a MC simulation of RT, radiation is simply handled as a collection of particles that individually interact with matter according to the basic laws of subatomic physics. For the modeling of body tissues, Schneider *et al* (2000) applied the stoichiometric approach to derive functions to convert a CT number directly to a mass density and elemental weights. The resultant functions for the particular scanning condition of their planning CT system are, however, not readily applicable to other planning CT systems or other scanning conditions (Vanderstraeten *et al* 2007). Calibration and maintenance of the complex one-to-many relations could discourage the practice of MC simulation. As well as for TP, MC simulation is potentially useful for detailed retrospective analysis of archived treatment plans, especially when they were partly planned with a retired CT system. In such cases, while the CT number may have been calibrated accurately against the primary ED, any other calibration may no longer be feasible.

To facilitate MC simulation for TP and for retrospective analysis, in this paper we extend the two-step approach to the derivation of mass density and elemental composition based on the latest compilation of standard tissue data. Accordingly, we also revise a CT-number conversion procedure currently in use for the first step of the two-step conversion. We compare the proposed conversion method with similar methods in the literature and demonstrate its implementation with a hypothetical planning CT system, primarily for proton and ion RT.

2. Materials and Methods

2.1. Standard tissues and material properties

We used the standard tissue data in ICRP Publication 110 (2009), which is the latest compilation of this kind. The publication offers the voxel representation of reference male and female phantoms structured with 141 organs, which are made of 53 standard tissues of enumerated mass density ρ and elemental weights w. The spongiosa tissues in the compilation may include mixing of the surrounding organ tissues such as trabecular bone, bone marrow and cartilage because their volumes could not be resolved due to the limited voxel resolution of the phantoms. For the ICRP-110 tissues, we derived electron density $n_{\rm e}$ by

$$n_{\rm e} = \frac{\rho}{u} \sum_i \frac{w_i Z_i}{A_{{\rm r}i}}, \tag{1}$$

where u is the unified atomic mass unit, Z_i is the atomic number and $A_{{\rm r}i}$ is the relative atomic mass for element i. We also derived stopping-power ratio S/S_w by

$$\frac{S}{S_{\rm w}} \approx \frac{n_{\rm e}}{n_{\rm ew}} \frac{\ln \frac{m_{\rm e}c^2}{I} - \frac{1}{3}}{\ln \frac{m_{\rm e}c^2}{I_{\rm w}} - \frac{1}{3}} \quad \text{with} \quad \ln I = \frac{\sum_i \frac{w_i Z_i}{A_{{\rm r}i}} \ln I_i}{\sum_i \frac{w_i Z_i}{A_{{\rm r}i}}}, \tag{2}$$

where subscript w indicates water, $m_{\rm e}c^2 = 511$ keV is the electron rest energy, $n_{\rm ew} = 3.343 \times 10^{23}$ cm^{-3} is the electron density of water, I_i is the mean excitation energy for element i in compounds (ICRU 1984) and $I_{\rm w} = 75.3$ eV is the I value consistently calculated for water (Kanematsu *et al* 2012). In the approximation, we adopted a typical ionizing-particle speed of $0.577\,c$ corresponding to a kinetic energy of 211 MeV for protons. We also derived tissue mass fraction m per person of an equal mixture of the male and female phantoms from the relevant organ masses.

As six major elements $M = \{$H, C, N, O, P, Ca$\}$ generally dominate the human body, we collected all other minor elements of each tissue into a residual weight and calculated its mean ($^-$) residual atomic number by

$$w_{\rm res} = \sum_{r \notin M} w_r \quad \text{and} \quad \bar{Z}_{\rm res} = \frac{\sum_{r \notin M} Z_r w_r}{w_{\rm res}}, \tag{3}$$

where Z_r is the atomic number of residual element r. The residual weight may be assigned to the element consistent with $\bar{Z}_{\rm res}$ to be reasonably included in MC simulation for general interactions.

2.2. Representative tissues

Among the ICRP-110 tissues, below $\rho = 0.90$ g/cm^3 was only a single lung tissue occupying $m = 1.4\%$ of the human body mass. Between 0.90 g/cm^3 and 1.00 g/cm^3 were an adipose tissue (33.9%) and medullary cavities containing bone marrow (0.4%). Between 1.00 g/cm^3 and 1.07 g/cm^3 were muscle (34.5%), spongiosa (0.3%) and many other general organ tissues (11.7%). Between 1.07 g/cm^3 and 1.101 g/cm^3 were

skin (4.9%), cartilage (0.6%) and spongiosa tissues (0.7%), which are miscellaneously epithelium, connective and spongy-bone tissues, respectively. Between 1.101 g/cm^3 and 1.25 g/cm^3 were only spongiosa tissues (5.7%). Above that were a mineral bone (5.7%) at 1.92 g/cm^3 and a tooth (0.1%) at 2.75 g/cm^3.

We hypothetically defined a representative tissue for each group (G) of tissues (t) in these density intervals by volume-weighted mean for the set ($\vec{\ }$) of densities $\vec{\rho} = (\rho, n_\mathrm{e}/n_\mathrm{ew}, S/S_\mathrm{w}, \rho_\mathrm{H}, \rho_\mathrm{C}, \rho_\mathrm{N}, \rho_\mathrm{O}, \rho_\mathrm{P}, \rho_\mathrm{Ca}, \rho_\mathrm{res})$ and by mass-weighted mean for the residual atomic number,

$$\vec{\rho}_G = \frac{\sum_{t\in G} \vec{\rho}_t \frac{m_t}{\rho_t}}{\sum_{t\in G} \frac{m_t}{\rho_t}} \quad \text{and} \quad \bar{Z}_{\mathrm{res}_G} = \frac{\sum_{t\in G} \bar{Z}_{\mathrm{res}_t} m_t}{\sum_{t\in G} m_t}, \tag{4}$$

where elemental density $\rho_{\{\mathrm{H,C,N,O,P,Ca,res}\}} = \rho\, w_{\{\mathrm{H,C,N,O,P,Ca,res}\}}$ is the mass density per element. In addition, we calculated the effective ($\tilde{\ }$) atomic numbers for the photoelectric effect and for coherent scattering of kV x-ray photons (Jackson and Hawkes 1981) by

$$\tilde{Z}_\mathrm{ph} = \left(\frac{\sum_i \frac{w_i Z_i}{A_{\mathrm{r}i}} Z_i{}^{3.62}}{\sum_i \frac{w_i Z_i}{A_{\mathrm{r}i}}} \right)^{\frac{1}{3.62}} \quad \text{and} \quad \tilde{Z}_\mathrm{coh} = \left(\frac{\sum_i \frac{w_i Z_i}{A_{\mathrm{r}i}} Z_i{}^{1.86}}{\sum_i \frac{w_i Z_i}{A_{\mathrm{r}i}}} \right)^{\frac{1}{1.86}} \tag{5}$$

for the stoichiometric CT-number calibration (Schneider *et al* 1996) that is used in many proton RT facilities.

2.3. Tissue segmentation and mixing

Compared to muscle and general organ tissues, adipose and marrow tissues have high concentrations of fat. Teeth have high concentrations of minerals and connective tissues have high concentrations of collagen, while bones lie between these two. The concentrations vary among and within individual tissues and are generally correlated with density. Therefore, an arbitrary tissue of mass density ρ can be regarded as a binary mixture of representative tissues 1 and 2 adjacent with higher and lower densities, or $\rho_1 \le \rho \le \rho_2$. In other words, by assigning the representative tissues to the polyline points, the mass density of a tissue in the polyline segment can be converted to the other densities by linear interpolation

$$\vec{\rho} = \frac{\rho_2 - \rho}{\rho_2 - \rho_1}\vec{\rho}_1 + \frac{\rho - \rho_1}{\rho_2 - \rho_1}\vec{\rho}_2 \tag{6}$$

in a mass-weighting manner (Warren *et al* 2015). When an ED $\tilde{\rho} \in \{n_\mathrm{e}/n_\mathrm{ew}, S/S_\mathrm{w}\}$ instead of the mass density is externally given to a tissue, the mixing weights in (6) may be redefined with replacement $\{\rho, \rho_1, \rho_2\} \to \{\tilde{\rho}, \tilde{\rho}_1, \tilde{\rho}_2\}$.

For air cavities, we added air of the standard atmosphere (ISO 1975) to the representative tissues. For fatty tissues lighter than the representative adipose/marrow tissue, we extended the soft-tissue segment down to fat of mass density 0.90 g/cm^3 at 37°C (Fidanza 2003) by adding the fat to the representative tissues. For the composition of the representative fat, we took 1,3-dioleoyl 2-palmitoyl glycerol (OPO triglyceride) found in human milk (Jenness 1979). Similarly, we extended the lung segment up to 0.80 g/cm^3, leaving a transition segment between 0.80 g/cm^3 and 0.90 g/cm^3 to

avoid discontinuity and to cope with fatty tissues that could accidentally be recognized as lighter than the representative fat. We also extended the tooth segment up to hydroxyapatite, the main component of tooth enamel, with a theoretical density of 3.156 g/cm^3 (Hench and Best 2013).

2.4. Comparison with preceding formulations

In contrast to our tissue-averaging approach, Schneider *et al* (2000) directly used air and seven selected tissues in another compilation (Woodard and White 1986) for CT-number conversion based on binary mixing of the tissue materials. We derived their implicit relations between mass and elemental densities, which we refer to as broken-line functions, each consisting of four disconnected segments. Using all tissues in the same compilation, Hünemohr *et al* (2014) formulated a relation between mass and electron densities consisting of two segments disconnected at 0.93 g/cm^3 of "Adipose 3", which we refer to as a bi-line function. We compared our polyline functions with those discontinuous functions.

2.5. New procedure for CT-number conversion

For CT-number conversion in the first step, we propose a new procedure of the stoichiometric calibration (Schneider *et al* 1996) as a revision of the one currently in use (Kanematsu *et al* 2003). The CT number H in Hounsfield unit (HU) is defined to be linearly related to photon attenuation coefficient μ as

$$H = 1000\,\frac{\mu-\mu_\mathrm{w}}{\mu_\mathrm{w}-\mu_\mathrm{a}} \approx 1001\left(\frac{\mu}{\mu_\mathrm{w}}-1\right), \tag{7}$$

where μ_w and $\mu_\mathrm{a} \approx 0.001\,\mu_\mathrm{w}$ are the μ values in water and in air. Based on the formulation by Jackson and Hawkes (1981), the photon attenuation coefficient in composite matter can be estimated (ˆ) by

$$\hat{\mu} = n_\mathrm{e}\,\sigma_\mathrm{C}\left(\kappa_\mathrm{ph}\tilde{Z}_\mathrm{ph}^{3.62}+\kappa_\mathrm{coh}\tilde{Z}_\mathrm{coh}^{1.86}+1\right), \tag{8}$$

where σ_C is the Compton-scattering cross section and $\kappa_\mathrm{ph}\tilde{Z}_\mathrm{ph}^{3.62}$ and $\kappa_\mathrm{coh}\tilde{Z}_\mathrm{coh}^{1.86}$ are the relative contributions of the photoelectric effect and of coherent scattering (Schneider *et al* 2000). The photon attenuation relative to that in water is thus given by

$$\frac{\hat{\mu}}{\hat{\mu}_\mathrm{w}} = \frac{n_\mathrm{e}}{n_\mathrm{ew}}\,\frac{\kappa_\mathrm{ph}\tilde{Z}_\mathrm{ph}^{3.62}+\kappa_\mathrm{coh}\tilde{Z}_\mathrm{coh}^{1.86}+1}{\kappa_\mathrm{ph}\tilde{Z}_{\mathrm{ph}_\mathrm{w}}^{3.62}+\kappa_\mathrm{coh}\tilde{Z}_{\mathrm{coh}_\mathrm{w}}^{1.86}+1}. \tag{9}$$

To determine the x-ray model parameters κ_ph and κ_coh, we followed Kanematsu *et al* (2003) to use specific-material samples for calibration. Table 1 shows their properties calculated with (1), (2) and (5). Measuring their μ/μ_w values by calibration CT scanning and substituting them for $\hat{\mu}/\hat{\mu}_\mathrm{w}$ in (9), the x-ray model parameters are solved to

$$\kappa_\mathrm{ph} = \frac{1}{\tilde{Z}_{\mathrm{ph}_\mathrm{w}}^{3.62}}\,\frac{\frac{\mu_\mathrm{K}}{\mu_\mathrm{w}}\frac{n_\mathrm{ew}}{n_\mathrm{eK}}\left(1-\frac{\tilde{Z}_{\mathrm{coh}_\mathrm{E}}^{1.86}}{\tilde{Z}_{\mathrm{coh}_\mathrm{w}}^{1.86}}\right)+\frac{\mu_\mathrm{E}}{\mu_\mathrm{w}}\frac{n_\mathrm{ew}}{n_\mathrm{eE}}\left(\frac{\tilde{Z}_{\mathrm{coh}_\mathrm{K}}^{1.86}}{\tilde{Z}_{\mathrm{coh}_\mathrm{w}}^{1.86}}-1\right)+\frac{\tilde{Z}_{\mathrm{coh}_\mathrm{E}}^{1.86}}{\tilde{Z}_{\mathrm{coh}_\mathrm{w}}^{1.86}}-\frac{\tilde{Z}_{\mathrm{coh}_\mathrm{K}}^{1.86}}{\tilde{Z}_{\mathrm{coh}_\mathrm{w}}^{1.86}}}{\frac{\mu_\mathrm{K}}{\mu_\mathrm{w}}\frac{n_\mathrm{ew}}{n_\mathrm{eK}}\left(\frac{\tilde{Z}_{\mathrm{coh}_\mathrm{E}}^{1.86}}{\tilde{Z}_{\mathrm{coh}_\mathrm{w}}^{1.86}}-\frac{\tilde{Z}_{\mathrm{ph}_\mathrm{E}}^{3.62}}{\tilde{Z}_{\mathrm{ph}_\mathrm{w}}^{3.62}}\right)+\frac{\mu_\mathrm{E}}{\mu_\mathrm{w}}\frac{n_\mathrm{ew}}{n_\mathrm{eE}}\left(\frac{\tilde{Z}_{\mathrm{ph}_\mathrm{K}}^{3.62}}{\tilde{Z}_{\mathrm{ph}_\mathrm{w}}^{3.62}}-\frac{\tilde{Z}_{\mathrm{coh}_\mathrm{K}}^{1.86}}{\tilde{Z}_{\mathrm{coh}_\mathrm{w}}^{1.86}}\right)+\frac{\tilde{Z}_{\mathrm{ph}_\mathrm{E}}^{3.62}}{\tilde{Z}_{\mathrm{ph}_\mathrm{w}}^{3.62}}\frac{\tilde{Z}_{\mathrm{coh}_\mathrm{K}}^{1.86}}{\tilde{Z}_{\mathrm{coh}_\mathrm{w}}^{1.86}}-\frac{\tilde{Z}_{\mathrm{ph}_\mathrm{K}}^{3.62}}{\tilde{Z}_{\mathrm{ph}_\mathrm{w}}^{3.62}}\frac{\tilde{Z}_{\mathrm{coh}_\mathrm{E}}^{1.86}}{\tilde{Z}_{\mathrm{coh}_\mathrm{w}}^{1.86}}}$$

Table 1. Material properties of samples for calibration CT scanning: mass density ρ, relative electron density n_e/n_{ew}, stopping-power ratio S/S_w, mean excitation energy I and effective atomic numbers $\tilde{Z}_{ph}$ for the photoelectric effect and $\tilde{Z}_{coh}$ for coherent scattering.

№	Material	$\rho/(g/cm^3)$	n_e/n_{ew}	S/S_w	I/eV	$\tilde{Z}_{ph}$	$\tilde{Z}_{coh}$
1	Water (H_2O)	0.997[a]	1	1	75.3	7.522	7.115
2	Ethanol (C_2H_5OH)	0.785[a]	0.801	0.817	63.1	6.497	5.984
3	40%-K_2HPO_4 solution	1.402[b]	1.344	1.300	99.2	12.506	10.555

[a,b]The mass densities are at 25°C ([a]OIML 1975, [b]Kanematsu *et al* 2003).

$$= \frac{1}{1487.1}\,\frac{0.20484\,\frac{\mu_K}{\mu_w} + 1.3514\,\frac{\mu_E}{\mu_w} - 1.3578}{0.10139\,\frac{\mu_K}{\mu_w} + 5.2635\,\frac{\mu_E}{\mu_w} - 3.3392} \tag{10}$$

and

$$\kappa_{coh} = \frac{1}{\tilde{Z}^{1.86}_{coh_w}}\,\frac{\frac{\mu_K}{\mu_w}\frac{n_{ew}}{n_{eK}}\left(\frac{\tilde{Z}^{3.62}_{ph_E}}{\tilde{Z}^{3.62}_{ph_w}} - 1\right) + \frac{\mu_E}{\mu_w}\frac{n_{ew}}{n_{eE}}\left(1 - \frac{\tilde{Z}^{3.62}_{ph_K}}{\tilde{Z}^{3.62}_{ph_w}}\right) + \frac{\tilde{Z}^{3.62}_{ph_K}}{\tilde{Z}^{3.62}_{ph_w}} - \frac{\tilde{Z}^{3.62}_{ph_E}}{\tilde{Z}^{3.62}_{ph_w}}}{\frac{\mu_K}{\mu_w}\frac{n_{ew}}{n_{eK}}\left(\frac{\tilde{Z}^{1.86}_{coh_E}}{\tilde{Z}^{1.86}_{coh_w}} - \frac{\tilde{Z}^{3.62}_{ph_E}}{\tilde{Z}^{3.62}_{ph_w}}\right) + \frac{\mu_E}{\mu_w}\frac{n_{ew}}{n_{eE}}\left(\frac{\tilde{Z}^{3.62}_{ph_K}}{\tilde{Z}^{3.62}_{ph_w}} - \frac{\tilde{Z}^{1.86}_{coh_K}}{\tilde{Z}^{1.86}_{coh_w}}\right) + \frac{\tilde{Z}^{3.62}_{ph_E}}{\tilde{Z}^{3.62}_{ph_w}}\frac{\tilde{Z}^{1.86}_{coh_K}}{\tilde{Z}^{1.86}_{oh_w}} - \frac{\tilde{Z}^{3.62}_{ph_K}}{\tilde{Z}^{3.62}_{ph_w}}\frac{\tilde{Z}^{1.86}_{coh_E}}{\tilde{Z}^{1.86}_{coh_w}}}$$

$$= \frac{1}{38.463}\,\frac{5.7101 - 0.30623\,\frac{\mu_K}{\mu_w} - 6.6149\,\frac{\mu_E}{\mu_w}}{0.10139\,\frac{\mu_K}{\mu_w} + 5.2635\,\frac{\mu_E}{\mu_w} - 3.3392}, \tag{11}$$

where subscripts E and K indicate ethanol and 40%-K_2HPO_4 solution, respectively.

The CT numbers of the representative tissues of known n_e, S/S_w, $\tilde{Z}_{ph}$ and $\tilde{Z}_{coh}$ will then be estimated by (7) and (9) to define the polyline relation between H and S/S_w. For CT-based MC simulation of proton or ion RT, the H–S/S_w relation will be applied to the first-step conversion and the invariant polyline relations between S/S_w and mass and elemental densities of the representative tissues will be applied in the second-step conversion. As a whole, the two-step conversion constitutes the function $\vec{\rho}(H)$ to estimate the set of densities for a given CT number H.

2.6. Example of two-step conversion

To demonstrate implementation of the two-step conversion, we theoretically emulated a CT system with hypothetical monochromatic 80-keV photons, which would effectively represent a kV x-ray spectrum, without realistic beam hardening or scatter contamination. While their remaining effects generally dominate the error in real CT imaging (Yang *et al* 2012), the hypothetical error-free CT may still suffice for this study dealing with the conversion part. For a material of known composition, the photon attenuation coefficient is theoretically given by

$$\mu = \sum_i \rho_i \left(\frac{\mu}{\rho}\right)_i, \tag{12}$$

where elemental mass attenuation coefficient $(\mu/\rho)_i$ for 80-keV photons is 0.3091 cm^2/g for H, 0.1610 cm^2/g for C, 0.1678 cm^2/g for O, 0.2324 cm^2/g for P and 0.3251 cm^2/g for K

(Hubbell and Selzer 2004). We used the theoretical calculation of (12) for calibration CT scanning to measure $\mu_{\rm E}/\mu_{\rm w} = 0.7839$ and $\mu_{\rm K}/\mu_{\rm w} = 1.612$, from which $\kappa_{\rm ph} = 2.248\times10^{-5}$ by (10) and $\kappa_{\rm coh} = 8.491 \times 10^{-4}$ by (11) were derived.

The accuracy of the CT-number conversion for tissues may intrinsically be limited by the accuracy of the model function of (9) calibrated with the samples, which we examined against the theoretical calculation of (12) with the database (Hubbel and Selzer 2004). We also compared the resultant H-to-$(S/\hat{S}_{\rm w})$ conversion function to that constructed with an old procedure by Kanematsu *et al* (2003), which was also directly derived from the same $\mu_{\rm E}/\mu_{\rm w}$ and $\mu_{\rm K}/\mu_{\rm w}$ values, though based on the tissue compilation in ICRU Report 46 (ICRU 1992). The polyline of the old procedure consisted of three segments for CT-number intervals: $[-1000, -600]$ HU for lung tissues, $[-150, 100]$ HU for soft tissues and $[300, 2000]$ HU for bone tissues and of two transition segments for $[-600, -150]$ HU and $[100, 300]$ HU. The accuracy of the overall conversion for MC simulation was examined by comparing the estimated densities $\vec{\hat{\rho}}(H)$ to the original densities $\vec{\rho}$ for the standard tissues and 24 additional tissues compiled in ICRU Report 44 (ICRU 1988), where CT number H was derived theoretically with (12) to emulate a CT scan with 80-keV photons. The ICRU-44 tissues were used in the original stoichiometric calibration (Schneider *et al* 1996) and have been considered as standard (Yang *et al* 2012).

3. Results

3.1. Tissue material properties

Table 2 shows the names and the material properties of the representative tissues. Figure 1 shows the correlation between mass density and relative electron density. The two fitting functions, the polyline of this study and the bi-line by Hünemohr *et al* (2014), were generally consistent with the standard tissues except around the representative fat at 0.90 g/cm^3 and around the representative tooth at 2.75 g/cm^3, where the bi-line function deviated by -1.5% and -1.3%, respectively. The discontinuity in the bi-line at 0.93 g/cm^3 was settled by the polyline.

Table 3 shows the elemental compositions of the representative tissues. Figure 2 shows the correlation between mass density and elemental densities. The polyline functions and the broken-line functions according to Schneider *et al* (2000) were both generally consistent with the standard tissues except between 1.0 g/cm^3 and 1.1 g/cm^3 for C, O and Ca, which were attributed to the light spongiosa tissues occupying 1% of the human body mass. Figure 3 shows the distribution of mean residual atomic number, where the highest and the lowest were 20.6 for the thyroid and 12.0 for the tooth, respectively. The global mean of 15.95 approximately corresponded to element S.

Table 2. Names and material properties of the representative tissues: mass fraction m, mass density ρ, relative electron density $n_{\mathrm{e}}/n_{\mathrm{ew}}$, stopping-power ratio S/S_{w}, mean excitation energy I and effective atomic numbers $\tilde{Z}_{\mathrm{ph}}$ for the photoelectric effect and $\tilde{Z}_{\mathrm{coh}}$ for coherent scattering.

№	Name	m/%	ρ/(g/cm^3)	$n_{\mathrm{e}}/n_{\mathrm{ew}}$	S/S_{w}	I/eV	$\tilde{Z}_{\mathrm{ph}}$	$\tilde{Z}_{\mathrm{coh}}$
1	Air		0.001	0.001	0.001	86.1	7.817	7.446
2	Lung	1.4	0.384	0.380	0.380	75.1	7.689	7.092
3	Extra Lung		0.80	0.793	0.794	75.1	7.689	7.092
4	Fat		0.90	0.906	0.928	61.3	5.952	5.553
5	Adipose/Marrow	34.3	0.950	0.952	0.968	64.9	6.516	6.000
6	Muscle/General	46.5	1.049	1.040	1.041	74.5	7.666	7.030
7	Miscellaneous	6.3	1.090	1.077	1.080	74.1	7.677	6.984
8	Heavy Spongiosa	5.7	1.136	1.115	1.116	75.1	9.600	7.691
9	Mineral Bone	5.7	1.92	1.784	1.705	109.7	13.75	11.59
10	Tooth	0.1	2.75	2.518	2.364	126.8	14.94	13.05
11	Hydroxyapatite		3.156	2.830	2.586	156.2	16.32	14.94

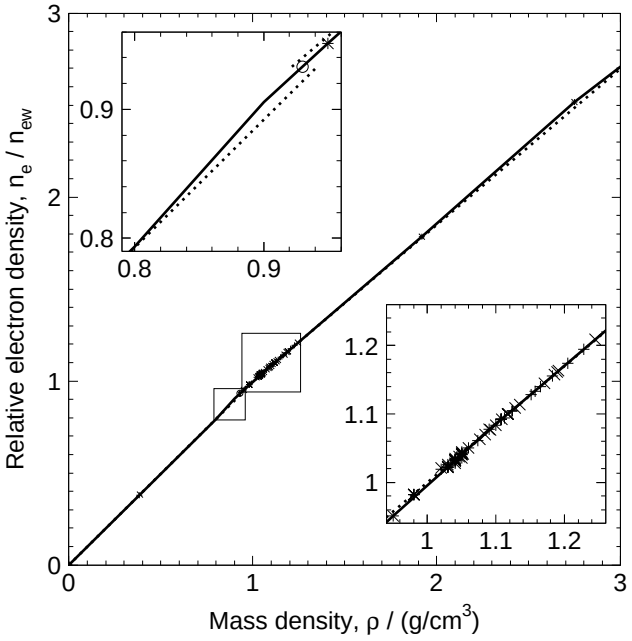

Figure 1. Relation between mass density and relative electron density for the ICRP-110 male (+) and female (×) tissues, the polyline function of this study (solid lines), the bi-line function (dashed lines) and "Adipose 3" (○) by Hünemohr *et al* (2014) and viewing areas for embedded subplots (rectangles).

3.2. CT-number conversion

Figure 4 shows the error of model-estimated $\hat{\mu}/\hat{\mu}_{\mathrm{w}}$ with respect to theoretical μ/μ_{w} of 80-keV photons. The error was typically as small as -0.003, while it was $+0.007$ for the thyroid. That may indicate the inaccuracy of the x-ray model calibrated with ethanol and 40%-K_2HPO_4 solution.

Table 3. Elemental composition of the representative tissues: major-element and residual weights $w_{\{\mathrm{H,C,N,O,P,Ca,res}\}}$ and mean residual atomic number $\bar{Z}_{\mathrm{res}}$.

№	Name	$w_{\mathrm{H}}/\%$	$w_{\mathrm{C}}/\%$	$w_{\mathrm{N}}/\%$	$w_{\mathrm{O}}/\%$	$w_{\mathrm{P}}/\%$	$w_{\mathrm{Ca}}/\%$	$w_{\mathrm{res}}/\%$	$\bar{Z}_{\mathrm{res}}$
1	Air	0.00	0.01	75.52	23.17	0.00	0.00	1.30	18.0
2	Lung	10.3	10.7	3.2	74.6	0.2	0.0	1.0	15.9
3	Extra Lung	10.3	10.7	3.2	74.6	0.2	0.0	1.0	15.9
4	Fat	11.96	76.87	0.00	11.17	0.00	0.00	0.00	—
5	Adipose/Marrow	11.40	58.92	0.74	28.64	0.00	0.00	0.30	14.7
6	Muscle/General	10.25	14.58	3.20	70.87	0.21	0.02	0.87	16.8
7	Miscellaneous	9.94	20.90	3.84	63.73	0.45	0.27	0.87	15.5
8	Heavy Spongiosa	9.30	39.15	2.22	41.71	2.36	4.60	0.66	14.9
9	Mineral Bone	3.6	15.9	4.2	44.8	9.4	21.3	0.8	13.1
10	Tooth	2.2	9.5	2.9	42.1	13.7	28.9	0.7	12.0
11	Hydroxyapatite	0.20	0.00	0.00	41.41	18.50	39.89	0.00	—

Figure 5 shows a comparison between the H-to-$(S/\hat{S}_{\mathrm{w}})$ conversion function of this study and that according to Kanematsu *et al* (2003), both of which were generally consistent with the stoichiometric tissue responses. The maximum deviation between the two $(S/\hat{S}_{\mathrm{w}})$ functions was 0.015 at 79 HU, which was due to their extended segmentation for soft tissues. Also, the deviation of $(S/\hat{S}_{\mathrm{w}})$ was typically 0.01 in their transition segments, where not many standard tissues exist.

Figure 6 shows the CT-number conversion functions for mass and elemental densities constructed with the two-step procedure for the hypothetical CT. These functions were generally consistent with the stoichiometric tissue responses except for the C, O and Ca densities in the CT-number interval of $[0, 100]$ HU, which were attributed to the light spongiosa tissues.

4. Discussion

The two-step approach for CT-number conversion offers distinct convenience for MC simulation of RT with multiple CT types and scan modes continually updated over time. The polyline-fitting approach may offer improved robustness against CT-number error or voxel averaging in a realistic CT image. The general agreement between the proposed and preceding formulations indicates their theoretical equivalence and the consistency of the tissue data, which is reasonable because all the relevant compilations are essentially based on an older compilation (ICRP 1975). Taking advantage of the publication that focused on reference adult phantoms rather than on variations in age, physical status, inter-individual, etc, the resultant concise yet complete set of the representative tissues may offer average tissue responses in general stoichiometric analysis. Yang *et al* (2012) estimated the proton range uncertainty due to deviation of an actual human body from the standard tissues to be 0.2% for lung, 1.2% for soft tissues and 1.6% for bones. Such errors in reality may only be assessed by *in vivo* dosimetric approaches (Mijnheer *et al*

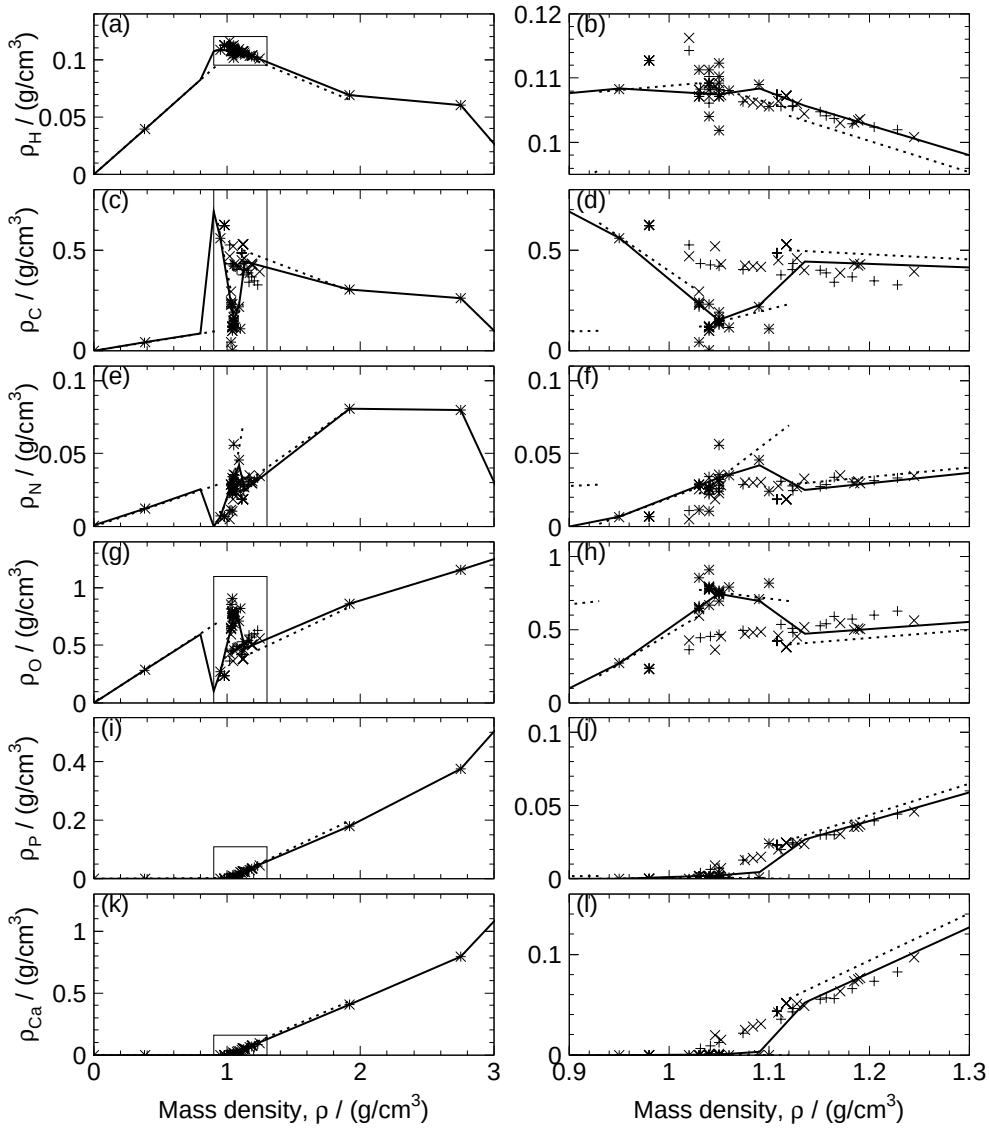

Figure 2. Relation between mass density and elemental densities of (a, b) H, (c, d) C, (e, f) N, (g, h) O, (i, j) P and (k, l) Ca for the ICRP-110 male (+) and female (×) tissues, the polyline functions of this study (solid lines), the broken-line functions according to Schneider *et al* (2000) (dashed lines) and viewing areas for next subfigures (rectangles).

2013, Knopf and Lomax 2013).

For CT-number conversion in the first step, we propose a new procedure with the same calibration apparatus as that currently used in multiple proton and ion RT facilities in Japan (Kanematsu *et al* 2003), where the transition will induce little impact on the management of planning CT systems. The simplicity and the clarity with minimum measurement of specific materials and with deterministic derivation of conversion relations are well maintained in the new procedure while naturally improving the accuracy with refined tissue segmentation with ten segments increased from five. In retrospective analysis of an archived treatment plan, the original ED distribution used

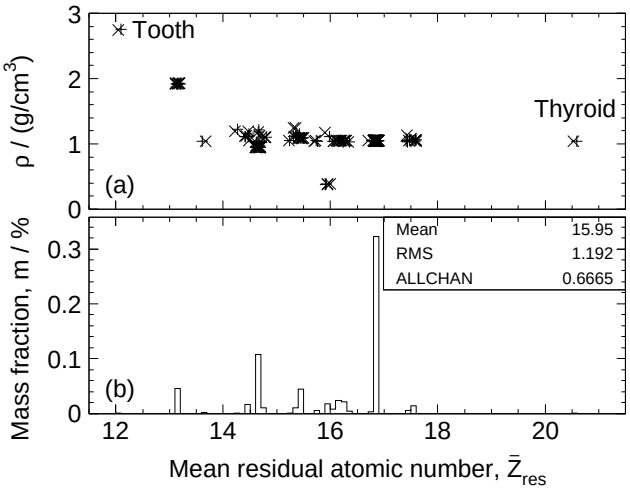

Figure 3. (a) Mean residual atomic number $\bar{Z}_{\rm res}$ versus mass density ρ for the ICRP-110 male (+) and female (×) tissues and (b) mass-weighted histogram of $\bar{Z}_{\rm res}$.

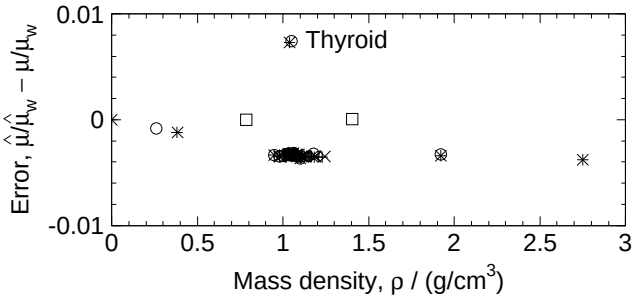

Figure 4. Mass density versus error of model-estimated relative attenuation $\hat{\mu}/\hat{\mu}_{\rm w}$ with respect to theoretical $\mu/\mu_{\rm w}$ of 80-keV photons for the ICRP-110 male (+) and female (×) tissues, the ICRU-44 tissues (○) and ethanol and 40%-K_2HPO_4 solution for calibration (□).

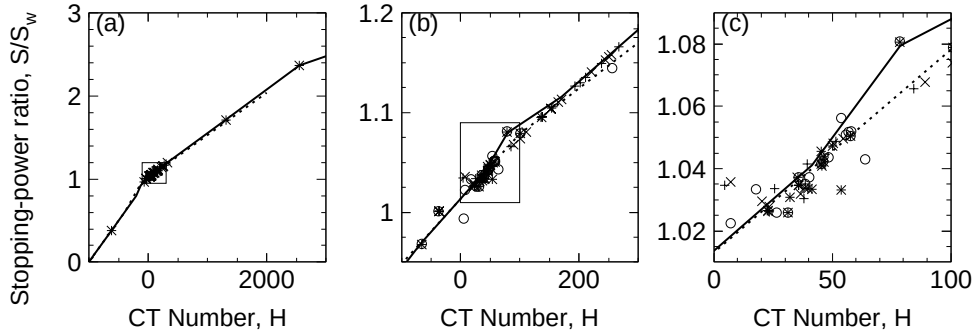

Figure 5. Relation between theoretical CT number with 80-keV photons and stopping-power ratio for the ICRP-110 male (+) and female (×) tissues, the ICRU-44 tissues (○), the conversion function of this study (solid line), the conversion function according to Kanematsu *et al* (2003) (dashed line) and viewing areas for next subfigures (rectangles).

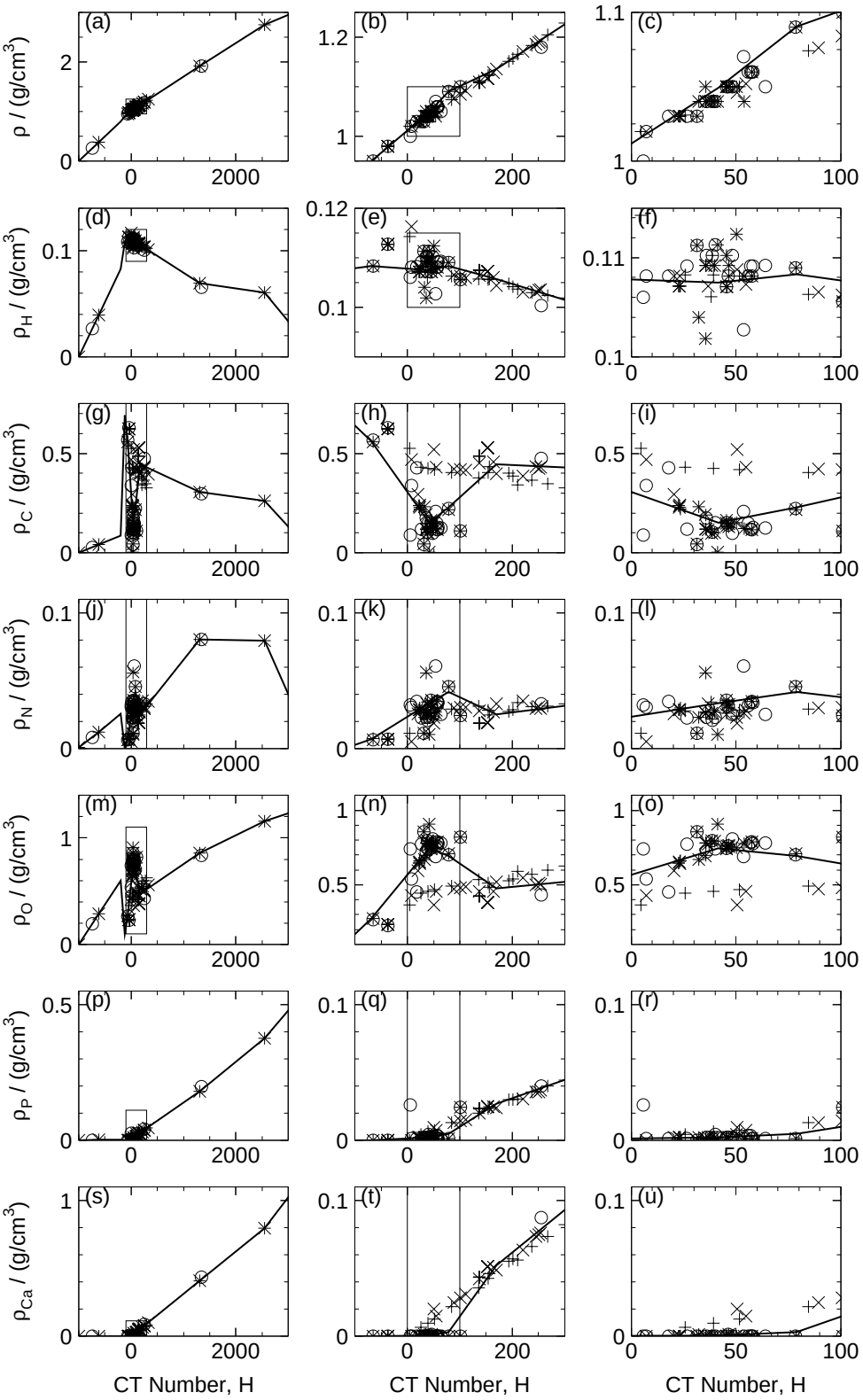

Figure 6. Relation between theoretical CT number for 80-keV photons in HU and (a–c) mass density and elemental densities of (d–f) H, (g–i) C, (j–l) N, (m–o) O, (p–r) P and (s–u) Ca for the ICRP-110 male (+) and female (×) tissues, the ICRU-44 tissues (○), the conversion functions (solid lines) and viewing areas for next subfigures (rectangles).

in TP may be readily available without redoing CT-number conversion.

The second-step inter-density conversion will lead to the mass density and elemental composition to constitute a patient model for subatomic MC simulation, where the residual mass may be assigned to element S or that consistent with $\bar{Z}_{\rm res}$ for the polyline segment. For accurate derivation of $\bar{Z}_{\rm res}$, the interpolation formula (6) should be applied to density-weighted parameter $\rho_{\rm res}\,\bar{Z}_{\rm res}$ from table 3. Similarly, when material properties I, $\tilde{Z}_{\rm ph}$ and $\tilde{Z}_{\rm coh}$ are needed for a given tissue, the interpolation parameters should be $n_{\rm e}\ln I$, $n_{\rm e}\,\tilde{Z}_{\rm ph}^{3.62}$ and $n_{\rm e}\,\tilde{Z}_{\rm coh}^{1.86}$ from table 2, with which the tissue receives the respective interactions. As an issue of MC implementation beyond this study, the conversion functions may have to be translated into numerical material data tables. In today's computing environment, material definition per CT number of a 12-bit integer to handle up to 4096 materials may sound practical, while Barnes *et al* (2013) showed that binning into 127 materials would still balance accuracy and efficiency.

With regard to the poor fitting for the elemental weights in the CT-number interval of [0,100] HU, the deviating light spongiosa tissues could be resolved by anatomical identification or by independent quantitative imaging, in which case either an extended spongiosa/mineral-bone segment or a separate marrow/spongiosa segment shall apply to the spongiosa tissues. The present estimation may be inaccurate for exceptional tissues such as thyroid, with its high iodine content, and for nonbiological materials such as artificial implants, for which specific material assignment is desirable. In recent years, dual-energy (DE) CT has been investigated for direct electron-density and atomic-number imaging, with which tissue types could be resolved (Bazalova *et al* 2008, Landry *et al* 2013). Some studies showed improvement with DECT over SECT in the absence of realistic image noise or artifacts: Yang *et al* (2010) theoretically showed that the root-mean-square error in stopping-power ratio remained below 1% with DE, as compared to 4% with SE, for non-standard tissues of perturbed density or composition. Hünemohr *et al* (2014) also estimated that range prediction would be improved by 0.1%–2.1% with DE. Tsukihara *et al* (2015) verified such improvements for electron-density measurement in phantoms. Nevertheless, further research and development may be needed to take advantage of DE in tomographic imaging of patient anatomy in the clinic. In fact, Landry *et al* (2013) showed that the advantage of DE in elemental-weight estimation would be insignificant at a CT dose index lower than 20 mGy or with a systematic error greater than 5 HU. Hudobivnik *et al* (2016) also questioned the significance of present-day DECT in TP for proton RT.

5. Conclusions

We defined 11 representative tissues for the human body as the materials specified by mass density and elemental composition and compiled their relative electron density, stopping-power ratio, mean excitation energy and effective atomic numbers for the photoelectric effect and for coherent scattering. These numerical tissues may be readily useful for general stoichiometric analysis. On the hypothesis that an arbitrary tissue is

a binary mixture of the representative tissues adjacent with higher and lower densities, its mass density, relative electron density and stopping-power ratio can be mutually converted by polyline interpolation. The elemental composition can be derived similarly via elemental densities. These relations were consistent with similar formulations in the literature and fitted to the standard tissues except for the C and O densities of the light spongiosa tissues occupying 1% of the human body mass.

For CT-based MC simulation of RT, we propose a two-step conversion method, in which these invariant relations are applied to inter-density conversion in the second step. For CT-number conversion in the first step, we revised a procedure practiced in multiple facilities, where the use of the same calibration apparatus will minimize the impact of the transition on the management of planning CT systems. The revised procedure also maintains the original simplicity and clarity while improving the accuracy by refined polyline segmentation. The two-step conversion was demonstrated to be practical using a theoretically emulated CT system and will facilitate MC simulation for TP and for retrospective analysis of archived treatment plans.

References

Barnes S, McAuley G, Slater J and Wroe A 2013 The effects of mapping CT images to Monte Carlo materials on GEANT4 proton simulation accuracy *Med. Phys.* **40** 041701-1–7

Bazalova M, Carrier J F, Bealieu L and Verhaegen F 2008 Dual-energy CT-based material extraction for tissue segmentation in Monte Carlo dose calculations *Phys. Med. Biol.* **53** 2439–56

Farace P 2014 Experimental verification of ion stopping power prediction from dual energy CT data in tissue surrogates *Phys. Med. Biol.* **59** 7081–4

Fidanza F 2003 Body fat in adult man: semicentenary of fat density and skinfolds *Acta Diabetol.* **40** s242–5

Fippel M and Soukup M 2004 A Monte Carlo dose calculation algorithm for proton therapy *Med. Phys.* **31** 2263–73

Hench L L and Best S M 2013 Ceramics, glasses, and glass-ceramics: basic principles *Biomaterials Science, Third Edition: An Introduction to Materials in Medicine* ed B D Ratner *et al* (*ISBN* 9780123746269) ch 1.2.4 pp 128–51 (San Diego, CA: Academic Press) p 141

Hubbell J H and Seltzer S M (2004) Tables of x-ray mass attenuation coefficients and mass energy-absorption coefficients, version 1.4 (*Standard Reference Database* 126) (Gaithersburg, MD: National Institute of Standards and Technology)

Hudobivnik N *et al* 2016 Comparison of proton therapy treatment planning for head tumors with a pencil beam algorithm on dual and single energy CT images *Med. Phys.* **43** 495–504

Hünemohr N, Paganetti H, Greilich S, Jäkel O and Seco J 2014 Tissue decomposition from dual energy CT data for MC based dose calculation in particle therapy *Med. Phys.* **41** 061714-1–14

ICRP 1975 *Report of the Task Group on Reference Man* (*Publication* 23) (Ottawa: International Commission on Radiological Protection)

ICRP 2009 *Adult Reference Computational Phantoms* (*Publication* 110) (Ottawa: International Commission on Radiological Protection)

ICRU 1984 *Stopping Powers for Electrons and Positrons* (*Report* 37) (Bethesda, MD: International Commission on Radiation Units and Measurements)

ICRU 1988 *Tissue Substitutes in Radiation Dosimetry and Measurement* (*Report* 44) (Bethesda, MD: International Commission on Radiation Units and Measurements)

ICRU 1992 *Photon, Electron, Proton and Neutron Interaction Data for Body Tissues* (*Report* 46) (Bethesda, MD: International Commission on Radiation Units and Measurements)

Inaniwa T, Kanematsu N, Hara Y and Furukawa T 2015a Nuclear-interaction correction of integrated depth dose in carbon-ion radiotherapy treatment planning *Phys. Med. Biol.* **60** 421–35

Inaniwa T, Kanematsu N, Tsuji H and Kamada T 2015b Influence of nuclear interactions in body tissues on tumor dose in carbon-ion radiotherapy *Med. Phys.* **42** 7132–7

Inaniwa T, Kanematsu N, Sato S and Kohno R 2016 A dose calculation algorithm with correction for proton-nucleus interactions in non-water materials for proton radiotherapy treatment planning *Phys. Med. Biol.* **61** 67–89

ISO 1975 *Standard Atmosphere* (*Standard* 2533) (Geneva: International Organization for Standardization)

Jackson D F and Hawkes D J 1981 X-ray attenuation coefficients of elements and mixtures *Phys. Rep.* **70** 169–233

Jenness R 1979 The composition of human milk *Semin. Perinatol.* **3** 225–39

Kanematsu N, Inaniwa T and Koba Y 2012 Relationship between electron density and effective densities of body tissues for stopping, scattering, and nuclear interactions of proton and ion beams *Med. Phys.* **39** 1016–20

Kanematsu N, Koba Y, Ogata R and Himukai T 2014 Influence of nuclear interactions in polyethylene range compensators for carbon-ion radiotherapy *Med. Phys.* **41** 071704-1–8

Kanematsu N, Matsufuji N, Kohno R, Minohara S and Kanai T 2003 A CT calibration method based on the polybinary tissue model for radiotherapy treatment planning *Phys. Med. Biol.* **48** 1053–64

Knopf A-C and Lomax A 2013 In vivo proton range verification: a review *Phys. Med. Biol.* **58** R131–60

Landry G, Parodi K, Wildberger E and Verhaegen F 2013 Deriving concentrations of oxygen and carbon in human tissues using single- and dual-energy CT for ion therapy applications *Phys. Med. Biol.* **58** 5029–48

Mijnheer B, Bedder S, Izewska J and Reft C 2013 In vivo dosimetry in external beam radiotherapy *Med. Phys.* **40** 070903-1–19

OIML 1975 *International Alcoholometric Tables* (*Recommendation* 22) (Paris: International Organization of Legal Metrology)

Schneider W, Bortfeld T and Schlegel W 2000 Correlation between CT numbers and tissue parameters needed for Monte Carlo simulation of clinical dose distributions *Phys. Med. Biol.* **45** 459–78

Schneider U, Pedroni E and Lomax A 1996 The calibration of CT Hounsfield units for radiotherapy treatment planning *Phys. Med. Biol.* **41** 111–24

Tsukihara M, Noto Y, Sasamoto R, Hayakawa T and Saito M 2015 Initial implementation of the conversion from the energy-subtracted CT number to electron density in tissue inhomogeneity corrections: An anthropomorphic phantom study of radiotherapy treatment planning *Med. Phys.* **42** 1378–88

Vanderstraeten B *et al* 2007 Conversion of CT numbers into tissue parameters for Monte Carlo dose calculations: a multi-centre study *Phys. Med. Biol.* **52** 539–62

Warren D R, Partridge M, Hill M A and Peach K 2015 Improved calibration of mass stopping power in low density tissue for a proton pencil beam algorithm *Phys. Med. Biol.* **60** 4243–61

Woodard H Q and White D R 1986 The composition of body tissues *Br. J. Radiol.* **59** 1209–1223

Yang M, Virshup G, Clayton J, Zhu X R, Mohan R and Dong L 2010 Theoretical variance analysis of single- and dual-energy computed tomography methods for calculating proton stopping power ratios of biological tissues *Phys. Med. Biol.* **55** 1343–62

Yang M, Zhu X R, Park P C, Titt U, Mohan R, Virshup G, Clayton J E and Dong L 2012 Comprehensive analysis of proton range uncertainties related to patient stopping-power-ratio estimation using the stoichiometric calibration *Phys. Med. Biol.* **57** 4095–115